Distributed Autonomous Guidance, Navigation and Control loop for Formation Flying Spacecraft Reconfiguration

Stefano Silvestrini, Vincenzo Pesce and Michèle Lavagna

Abstract This paper presents a continuous low-thrust control algorithm coupled with the decentralized navigation filter, suitable for distributed space systems reconfiguration. The dynamics of the satellites, representative of J2-perturbed elliptical orbits, is expressed in terms of the relative orbital elements (ROEs). Since the relative orbit determination measurements are typically referred to the Cartesian state of each satellite, a linear mapping between the set of ROE and the Cartesian coordinates expressed in the local-vertical-local-horizontal (LVLH) reference frame is derived. The desired set of ROE at each time-step is determined based on the contribution of counter-acting Artificial Potential Fields (APFs) defined in the ROE space. A feedback control is designed to track the desired state, whose stability is analysed using Lyapunov theory. The guidance, navigation and control algorithms are tested in a high-fidelity numerical orbit propagator for two different operational scenarios, one of which is accurately chosen to show a representative collision avoidance manoeuvre. The results demonstrate the effectiveness of the algorithm for reconfiguration manoeuvres involving relative distances $\sim 10^2$ m with limited fuel consumption and constrained available thrust ($\leq 1mN$). The proposed algorithm enhances the flexibility of traditional reconfiguration with collision avoidance strategies respecting the robustness requirement and the computational effort.

Stefano Silvestrini
PhD Cadidate
Politecnico di Milano, Via La Masa 34, 20156, Milano e-mail: stefano.silvestrini@polimi.it

Vincenzo Pesce
PhD Candidate
Politecnico di Milano, Via La Masa 34, 20156, Milano e-mail: vincenzo.pesce@polimi.it

Michèle Lavagna
Associate Professor
Politecnico di Milano, Via La Masa 34, 20156, Milano e-mail: michelle.lavagna@polimi.it

1 Introduction

Distributed space systems, composed of several microsatellites flying in formation, are becoming increasingly attractive due to the resulting enhancement in robustness of the overall mission architecture while reducing the cost of each platform and the time to flight. The Guidance, Navigation & Control (GNC) subsystem of the fractionated space system is required to drive and keep the microsatellites formation towards multiple different configurations, which are imposed by the mission objectives. A high-level of autonomy, and consequently increased complexity, is required in such mission concept, in which the satellites are expected to react autonomously to unforeseen events. In particular, the collision avoidance task is critical in formation reconfiguration especially when the number of satellites increases. The GNC algorithms can be implemented following a centralized, decentralized or distributed architecture. The centralized architecture assumes there is a master spacecraft that processes the information coming from all the satellites, computes the guidance and control outcome and sends back commands to each spacecraft [5]. Decentralized GNC implements identical algorithms on-board each satellite, which is capable of computing its own action based solely on on-board information [10]. Finally, distributed systems relies on inter-satellite links: indeed, each satellite processes its own information and at least one coming from another agent of the system [2]. On one hand, the centralized architecture presents two different issues: first, the presence of a master spacecraft implies a single failure point; the outcome of the central on-board calculation needs to be circulated among all the agents of the system, inserting complexity on the communication link between the master and the other spacecrafts. The decentralized approach, on the other hand, solves the failure point aspect but lacks of a system perception, as each satellite is limited to its own data. For this reason, the selected architecture for this paper is distributed, which aims at solving the aforementioned issues of the centralized and decentralized approach. Even though formation flying missions are not so numerous, in literature [2] [5] the path-planning is an optimum problem solved for the trajectory of each satellite taking into account the collision hazard constraint of the constructed trajectories. Both centralized and distributed architecture have been studied [2]. Nevertheless, this might become computationally demanding as the number of satellites increases, especially when on board computational resources are very limited. Di Mauro et al. [5] presented an optimal continuous control law for satellite reconfiguration, solved by Mixed Linear Programming and Particle Swarm Optimization. Such approach is hardly fitting the constraints imposed by the micro-platforms and does not take into account any collision avoidance strategy. The collision constraint has been taken into account in the optimal control strategy presented by Chu [2], by convexifying the constraint solved by nonlinear programming strategy. Nevertheless, the navigation algorithm is not integrated nor developed. Chernick et al. [1] presented an optimal control based on impulsive maneuver leveraging Keplerian dynamics to determine optimal, predictable maneuvering schemes, without taking into account the collision avoidance constraint. An impulsive strategy based on the state transition matrix of the system is also presented by Vadali and Alfriend [15]. Schaub [11]

presented a low-thrust feedback law based on orbital elements difference valid for Cartesian J2-invariant orbits. Another formation control strategy for reconfiguration is using the virtual-structure approach (VSA). Basically, the final configuration is associated to a rigid frame in which the satellites are pre-assigned to a specific place, which is tracked by each satellite's control architecture. Ren et al. [10] proposed a decentralized scheme for spacecraft Formation Flying using the VSA. Several authors have partially solved the task of path-planning using behaviour-based algorithms. Izzo [7] presented a behaviour-based algorithm, where the imposed desired velocity is determined by a combination of counteracting task, such collision avoidance and reference tracking. The Null-Space Based (NSB) behavioral control concept is used by Schlanbusch [13] to cope with the dynamic collision avoidance constraint, coupled with a sliding surface based controller. Similar to the behaviour-based approach is the calculation of the artificial potential field to force the dynamics of the agents during the reconfiguration. Steindorf et al. [14] proposed a guidance and control strategy based on the artificial potential field using relative orbital elements. The authors include a passive collision avoidance strategy applicable to satellite formations composed of two satellites. The relative elements adopted in this paper are the same developed by D'Amico [3] and used also by Steindorf [14]. The relative motion between spacecrafts flying in formation is typically reconstructed by Cartesian measurement in the Hill frame. Hence, a linear mapping is developed to transform the Cartesian state to the relative orbital elements $\delta \chi$, and vice versa. A similar approach was developed by Schaub [12], where the mean orbital elements difference were used. The literature is still poor with respect to algorithms that can be implemented in a distributed architecture with low computational power, actively managing the collision avoidance constraint between more than two satellites. As stated, this paper presents an autonomous formation reconfiguration GNC algorithm based on artificial potential field, including a distributed active collision avoidance based on repulsive potential contribution, suitable for microsatellite applications. A tracking feedback controller, based on Lyapunov theorem, guarantees the artificial potential dynamics to be followed. The intended contributions of the paper are:

- to propose a full GNC algorithm for spacecrafts formation reconfiguration, suitable for micro platforms implementation;
- to extend the application of the artificial potential field to dynamically control multiple agents (≥ 2) assuring the collision avoidance constraint is respected;
- to develop a numerical tool to test and validate the full GNC algorithm.

The paper is structured as follows: the dynamical model employed and the coordinates transformation are presented in section 2; in section 3 the full GNC architecture is detailed, with dedicated focus to the distributed guidance, navigation and control algorithms. The numerical simulations and results are reported in section 4; finally, in section 5, conclusions are drawn.

2 Dynamical Model

The spacecraft formation dynamics is described using the relative orbital elements, following the work done by D'Amico [3]. The following quasi-singular relative orbital elements are adopted:

$$
\delta\chi = \begin{pmatrix} \delta a \\ \delta\lambda \\ \delta e_x \\ \delta e_y \\ \delta i_x \\ \delta i_y \end{pmatrix} = \begin{pmatrix} \frac{a_f - a_r}{a_r} \\ (M_f + \omega_f) - (M_r + \omega_r) + (\Omega_f - \Omega_r)\cos(i_r) \\ e_f\cos(\omega_f) - e_r\cos(\omega_r) \\ e_f\sin(\omega_f) - e_r\sin(\omega_r) \\ i_f - i_r \\ (\Omega_f - \Omega_r)\sin(i_r) \end{pmatrix}
\tag{1}
$$

where the subscript f stands for any follower spacecraft orbit, whereas the subscript indicates the reference orbital elements. M is the mean anomaly, a the semimajor axis, e the eccentricity, i the orbit inclination, ω the argument of perigee and Ω the right ascension of the ascending node. It is important to remark that in this paper the reference orbit is the same for the n spacecraft building up the formation. The benefit of using such model is that, if the perturbations are neglected, the geometry of the relative motion with respect to a reference orbit is uniquely determined by a set of invariant relative orbital elements (ROE), except for the relative true anomaly, which follows the Keplerian propagation. Indeed, the natural evolution of the dynamic system can be described as:

$$
\dot{\delta\chi} = A_k \cdot \delta\chi
\tag{2}
$$

where

$$
A_k = \begin{bmatrix} 0 & \vdots & \\ -1.5n & \vdots & \mathbf{0}_{6\times 5} \\ \mathbf{0}_{4\times 1} & \vdots & \end{bmatrix}
\tag{3}
$$

Guffanti and Koenig [6][8] later expanded the model to a J_2 perturbed dynamics. The complete dynamical model can be expressed as:

$$
\dot{\delta\chi} = (A_k + A_{J2}) \cdot \delta\chi + B\mathbf{u}
\tag{4}
$$

$$
A_{J_2} = \begin{bmatrix} 0 & 0 & 0 & 0 & 0 \\ -\frac{7}{2}(1+\eta)(3\cos^2 i_r - 1) & 0 & e_x GFP & e_y GFP & -FS & 0 \\ \frac{7}{2}e_y Q & 0 & -4e_x e_y GQ & -(1+4Ge_y^2)Q & 5e_y S & 0 \\ -\frac{7}{2}e_x Q & 0 & (1+4Ge_x^2)Q & 4e_x e_y GQ & -5e_x S & 0 \\ 0 & 0 & 0 & 0 & 0 & 0 \\ \frac{7}{2}S & 0 & -4e_x GS & -4e_y GS & 2T & 0 \end{bmatrix}
\tag{5}
$$

where the terms in Eq. 5 are:

$$k = \gamma a_r^{-\frac{7}{2}} \eta^{-4}, \ \eta = \sqrt{1 - e_r^2}, \ \gamma = \frac{3}{4} J_2 R_e^2 \sqrt{\mu}, \ e_x = e_r \cos \omega_r, \ e_y = e_r \sin \omega_r$$

$$E = 1 + \eta, \ G = \frac{1}{\eta^2}, \ F = 4 + 3\eta, \ P = 3\cos^2 i_r - 1, \ Q = 5\cos^2 i_r - 1, \ S = \sin 2i_r, \ T = \sin^2 i_r \tag{6}$$

where $J2$ is the zonal harmonic coefficient $1.0826 \cdot 10^{-3}$ for Earth, R_e is the Earth radius, $\mu = 3.986 \cdot 10^{14} m^3 s^{-2}$ is the Earth gravitational constant. The control matrix is derived from Gauss Variational Equation (GVE) as in [11]:

$$B = \frac{1}{a_r n_r} \begin{bmatrix} \frac{2}{\eta} e_r \sin v_r & \frac{2}{\eta}(1 + e_r \cos v_r) & 0 \\ -\frac{2\eta^2}{1 + e_r \cos v_r} & 0 & 0 \\ \eta_r \sin \omega_r + v_r & \eta \frac{(2 + e_r \cos v_r)\cos(\omega_r + v_r) + e_x}{1 + e_r \cos v_r} & \frac{\eta e_y}{\tan i_r} \frac{\sin(\omega_r + v_r)}{1 + e_r \cos v_r} \\ -\eta_r \cos \omega_r + v_r & \eta \frac{(2 + e_r \cos v_r)\sin(\omega_r + v_r) + e_y}{1 + e_r \cos v_r} & \frac{-\eta e_x}{\tan i_r} \frac{\sin(\omega_r + v_r)}{1 + e_r \cos v_r} \\ 0 & 0 & \eta \frac{\cos(\omega_r + v_r)}{1 + e_r \cos v_r} \\ 0 & 0 & \eta \frac{\sin(\omega_r + v_r)}{1 + e_r \cos v_r} \end{bmatrix} \tag{7}$$

where v_r is the true anomaly.

2.1 Coordinates Transformation

The active collision avoidance maneuvers depend on the relative metric distance between two agents. The relative distance is naturally expressed in the Cartesian Local-Vertical-Local-Horizontal (LVLH) reference frame. The mapping between the Hill $\mathbf{X} = [x \ y \ z \ \dot{x} \ \dot{y} \ \dot{z}]$ state to the ROE $\delta \chi$ is required to process the measurements and compute the guidance and control output. The transformation matrices are derived by using the classical orbital elements difference $\Delta OE = [\Delta a \ \Delta M \ \Delta \omega \ \Delta e \ \Delta i \ \Delta \Omega]$ as follows:

$$J_{\delta \chi}^X = \frac{\partial \mathbf{X}}{\partial \Delta OE} \cdot \frac{\partial \Delta OE}{\partial \delta \chi}, \quad J_X^{\delta \chi} = \frac{\partial \delta \chi}{\partial \Delta OE} \cdot \frac{\partial \Delta OE}{\partial \mathbf{X}} \tag{8}$$

where a is the semimajor axis, M is the mean anomaly, ω the argument of perigee, e the eccentricity, i the inclination and Ω the right ascension of the ascending node. The first-order approximation of the mapping between the Hill state and classical osculating orbital elements yields [3][9]:

$$x = \frac{r}{a} \Delta a - a \cdot \cos v \Delta e + \frac{ae \sin v}{\sqrt{1 - e^2}} \Delta M$$

$$y = \left(a + \frac{r}{1 - e^2} \right) \sin v \Delta e + \frac{a^2}{r} \eta \Delta M + r \Delta \omega + r \cos i \Delta \Omega \tag{9}$$

$$z = r \sin(v + \omega) \Delta i - r \sin i \cos(v + \omega) \Delta \Omega$$

Differentiating Eq. 9 the full transformation is obtained:

$$\dot{x} = -\frac{ne\sin\nu}{2\sqrt{1-e^2}}\Delta a + n\sin\nu\sqrt{1-e^2}\left(\frac{a^3}{r^2}\right)\Delta e + en\cos\nu\frac{a^3}{r^2}\Delta M$$

$$\dot{y} = \left[n\sqrt{1-e^2}\left(1+\frac{r}{a(1-e^2)}\right)\left(\frac{a^3}{r^2}\right)\cos\nu + \frac{aen\sin^2\nu}{(1-e^2)^{\frac{3}{2}}}\right]\Delta e - en\sin\nu\frac{a^3}{r^2}\Delta M + \frac{aen\sin\nu}{\sqrt{1-e^2}}\Delta\omega$$

$$\dot{z} = \frac{an}{\sqrt{1-e^2}}\left(\sin i\left[\sin(\nu+\omega)+e\sin\omega\right]\Delta\Omega + \left[\cos(\nu+\omega)+e\cos\omega\right]\Delta i\right)$$

$$\tag{10}$$

Combining Eq. 9 and 10 the transformation matrix between Hill state $\mathbf{X}$ and classical orbital elements ΔOE, namely $\frac{\partial\mathbf{X}}{\partial\Delta OE}$ and its inverse in Eq. 8. To formulate the complete transformation the Jacobian of the transformation between classical orbital elements and relative orbital elements $\delta\chi$ is required. Such transformation is obtained from the definition of $\delta\chi$ for $\Delta OE \to 0$:

$$\frac{\partial\Delta OE}{\partial\delta\chi} = \begin{bmatrix} a & 0 & 0 & 0 & 0 & 0 \\ 0 & 1 & \frac{\sin\omega}{e} & -\frac{\cos\omega}{e} & 0 & \frac{\cos i}{\sin i} \\ 0 & 0 & -\frac{\sin\omega}{e} & \frac{\cos\omega}{e} & 0 & 0 \\ 0 & 0 & \cos\omega & \sin\omega & 0 & 0 \\ 0 & 0 & 0 & 0 & 1 & 0 \\ 0 & 0 & 0 & 0 & 0 & \sin i \end{bmatrix}, \quad \frac{\partial\delta\chi}{\partial\Delta OE} = \begin{bmatrix} \frac{1}{a} & 0 & 0 & 0 & 0 & 0 \\ 0 & 1 & 1 & 0 & 0 & \cos i \\ 0 & 0 & -e\sin\omega & \cos\omega & 0 & 0 \\ 0 & 0 & e\cos\omega & \sin\omega & 0 & 0 \\ 0 & 0 & 0 & 0 & 1 & 0 \\ 0 & 0 & 0 & 0 & 0 & \sin i \end{bmatrix}$$

$$\tag{11}$$

3 Distributed Architecture

The entire Guidance, Navigation & Control is designed according to a distributed architecture, in which each satellite processes the information coming from its neighbouring satellite. Each satellite processes on-board the information on its state together with the relative measurements of its neighbour. As mentioned, the collision avoidance maneuver is calculated on-board based on the relative distance between satellites. This is done on-board and actively calculated as the satellites are moving, which is different from what has been done in literature. The implementation of the proposed algorithm is independent from the number of satellites in the system. In the following the approach adopted for each GNC block, Navigation, Guidance and then Control, is detailed.

3.1 Decentralized Navigation

The navigation strategy exploits a decentralized architecture. In this way, the highly parallel nature of this solution allows for a much faster implementation, especially with a high number of satellites in the formation. The navigation algorithm is the same for all the satellites in the formation. Each satellite is assumed to be able to retrieve its relative state with respect to the reference orbit. This can be achieved exploiting the information from cameras or by radio frequency (RF) communication. In this work, we assume to use a relative RF communication as in Prisma mission did[4]. The output of the RF signal analysis is directly the relative position vector between the two spacecrafts. This measurement is fed to the navigation filter. We implemented a standard Kalman Filter (KF) to estimate the relative position and velocity between each satellite and a reference satellite of the formation that is the only one able to estimate its absolute state, which can be performed by any satellite of the formation. The algorithm is implemented identically for each spacecraft in the formation and it is independent of the other satellites. The particular formulation of the dynamics with ROE allows to use a linear estimator. This is very important to limit the computational effort while preserving the estimation performance. It is worth underlying that the state vector of the filter is composed by the Hill state $\mathbf{X} = [x\ y\ z\ \dot{x}\ \dot{y}\ \dot{z}]$ and not ROE. This strongly simplifies the tuning of the filter but implies an additional conversion downstream of the navigation block to correctly execute the guidance algorithms.

3.2 Distributed Guidance

The distributed guidance algorithm processes locally all the state estimations of the satellite formation members. The leader satellite owns a full knowledge of the system, hence relative distances between followers are available. The guidance strategy relies on artificial potential functions designed in the relative orbital elements space in $\mathbb{R}^6$. The idea is to build a point-wise global potential based on the contribution of attractive and repulsive potential sources, namely the target relative orbits and any other satellite located in close neighbouring areas. The attractive potential is directly expressed in terms of relative orbital elements, those being a convenient way to express relative orbits geometry. Indeed, a set of relative orbital elements uniquely define one particular formation configuration. On the other hand, the natural way to express the vicinity between two satellites is using the Cartesian distance, expressed in the LVLH reference frame in this particular application. To obtain a uniform expression of the global potential, the Jacobian of the transformation is derived, based on the results presented in sec. 2.1. The output of the guidance, for each satellite, is what we call *guidance state* and indicate as $\delta\chi_g$. The guidance algorithm forces the following dynamics for each satellite i:

$$\dot{\delta\chi_{\mathbf{g}}} = -\nabla\Phi_{glb} \qquad (12)$$

where Φ_{glb} is the global potential:

$$\nabla \Phi_{glb} = \nabla \Phi_a + \nabla \Phi_r \tag{13}$$

where Φ_a is the attractive potential, whereas Φ_r is the repulsive one. The reconfiguration objective is to drive the satellites to a predefined relative configuration, expressed in term of relative orbital elements. The set of ROE to be achieved are called *reference state* and indicated as $\delta\chi_r$. The attractive contribution to the global potential is determined as:

$$\Phi_a(\delta\chi) = \frac{1}{2}\xi_a \left\| \delta\chi_g - \delta\chi_r \right\|^2 \tag{14}$$

The gradient in the guidance ROE space is defined as:

$$\nabla_{\delta\chi_g}(\cdot) = \left(\frac{\partial}{\partial \delta a}, \frac{\partial}{\partial \delta \lambda}, \frac{\partial}{\partial \delta e_x}, \frac{\partial}{\partial \delta e_y}, \frac{\partial}{\partial \delta i_x}, \frac{\partial}{\partial \delta i_y} \right)_g \tag{15}$$

Consequently, the dynamic contribution to Eq. 13 given by the attractive potential is:

$$\nabla_{\delta\chi_g} = \xi_a(\delta\chi_g - \delta\chi_r) \tag{16}$$

Active Collision Avoidance

The repulsive potential is useful to calculate the trajectory in presence of other satellites, avoiding collision between agents. As previously stated, to achieve an efficient active collision avoidance maneuver, the potential is best representative in terms of the Cartesian state X in the Hill frame, where the metric distance is defined. Given two satellites, i and j respectively, the repulsive potential to be computed for Eq. 13 for satellite i is defined as:

$$\Phi_{r_{ij}} = \begin{cases} \frac{1}{2}\xi_r e^{-\frac{d_{ij}^2}{\eta}} = \frac{1}{2}\xi_r e^{-\frac{\|x_i - x_j\|^2}{\eta}} & \text{if } d_{ij} < d_{lim}, \\ 0 & \text{if } d_{ij} > d_{lim} \end{cases} \tag{17}$$

where d_{lim} is the threshold distance beyond which the collision maneuver is not required. In the centralized configuration, the state of the position of the spacecrafts is known, thus it is possible to calculate the distance vector as the difference between $X_i - X_j$. The gradient of the potential is calculated using the chain-rule, which involves the coordinate transformation from Cartesian state X to ROE $\delta\chi$:

$$\nabla_{\delta\chi_g} \Phi_{r_{ij}} = \nabla_X \Phi_{r_{ij}} \cdot J_{\delta\chi}^X \tag{18}$$

where $J_{\delta\chi}^X$ is the Jacobian of the coordinate transformation, derived in section 2.1. The gradient in the Cartesian space is defined as:

$$\nabla_X(\cdot) = \left(\frac{\partial}{\partial x}, \frac{\partial}{\partial y}, \frac{\partial}{\partial z} \right) \tag{19}$$

Hence, the gradient of the repulsive potential between agents i and j, below the threshold, can be expressed as:

$$\nabla_{\delta\chi_g} \Phi_{r_{ij}} = -\frac{\xi_r}{\eta} e^{-\frac{d_{ij}^2}{\eta}} \cdot (\boldsymbol{X_i} - \boldsymbol{X_j}) \cdot J_{\delta\chi}^X \tag{20}$$

The repulsive potential takes into account all the mutual distances between the formation agents; coherently, the repulsive contribution to the global potential for satellite i is the summation of the mutual repulsive potential between satellite i and all the other satellites:

$$\Phi_r = \sum_{j \neq i}^{n} \Phi_{r_{ij}} \tag{21}$$

where n is the number of spacecrafts in the formation.

3.3 Distributed Control

The output of the guidance algorithm is a set of ROE, which may differ from the target reference ones. To guarantee that the forced guidance dynamics in Eq. 12 is followed, a feedback control law is employed. The control law is derived using the Lyapunov stability theorem. In the centralized architecture, the leader processes the guidance loop for the entire formation as well as the calculation of the control input for each satellite, which is then actuated by each agent. The reference signal to track is calculated by the guidance algorithm and follows the dynamics in Eq. 12. The current error between the desired guidance state and true state, for the entire formation, is:

$$\boldsymbol{e}_{\delta\chi} = \delta\chi_g - \delta\chi \tag{22}$$

its temporal evolution can be described as:

$$\dot{\boldsymbol{e}}_{\delta\chi} = \delta\dot{\chi}_g - \delta\dot{\chi} = -\left(\nabla\Phi_a + \nabla\Phi_r \right) - \left(A(v)\delta\chi + B\boldsymbol{u} \right) \tag{23}$$

If we introduce the following positive semi-definite Lyapunov function:

$$V = \frac{1}{2}\mathbf{e}_{\delta\chi}^T \mathbf{e}_{\delta\chi} \rightarrow \dot{V} = \mathbf{e}_{\delta\chi}^T \dot{\mathbf{e}}_{\delta\chi} \tag{24}$$

$$\dot{V} = \left(\delta\chi_g - \delta\chi \right) \cdot \left[-\left(\nabla\Phi_a + \nabla\Phi_r + A(v)\delta\chi + B\boldsymbol{u} \right) \right] \tag{25}$$

The control term can be solved to make the derivative of the Lyapunov function negative. The aim is to drive the derivative to the term $-\mathbf{e}_{\delta\chi}^T\mathbf{e}$, which is always negative. Hence, the following control law is derived:

$$\boldsymbol{u} = B^{-1}\left[\left(\delta\chi_g - \delta\chi\right) - \left(\nabla\Phi_a + \nabla\Phi_r\right) - A(\nu)\delta\chi\right] \qquad (26)$$

In this way the derivative of the Lyapunov function is negative semi-definite, vanishing only when $\delta\chi = \delta\chi_r$, which is within the validity of the Lyapunov theorem. This approach is similar to the one adopted by Steindorf [14], with the exception of including the gradient of artificial potential in the control law. By including the gradient of the potential, which forces the dynamics, the control law calculates the action taking into account the derivative of the $\delta\chi_g$ determined by the guidance algorithm. The repulsive potential field incorporates the measurements of relative distances between the agents, yielding a distributed architecture. Each spacecraft completes the GNC loop requiring at least one relative distance measurement with respect to another agent.

3.4 GNC algorithm overview

The full GNC loop described in section 3.1, 3.2 and 3.3. The algorithm workflow is:

1. Acquisition of states measurement by each satellite;
2. The measurements are filtered to obtain a refined state vector;
3. Determination of the relative neighbouring states $\mathbf{r}_{ij}$ and $\mathbf{v}_{ij}$;
4. Calculation of the artificial potential field Φ_{glb} and the corresponding gradient $\nabla\Phi_{glb}$ to establish the forced reconfiguration dynamics on-board each satellite based on the relative measurements;
5. Calculation of the the control effort $\mathbf{u}$, subject to thrust constraints, on-board each satellite.

A schematic of the block diagram of the full GNC architecture is sketched in Fig. 1. The Kalman Filter is implemented in a decentralized architecture; the filter processes relative state measurement with respect to the reference orbit. The relative measurements between neighbouring satellites are directly fed to the guidance calculation. The guidance block calculates the desired $\delta\chi_g$ based on the generation of the artificial potential field, which is comprehensive of the repulsive action of the neighbouring satellites. The aim of the guidance forced dynamics is to drive the spacecraft to the desired relative orbit preventing the satellites from colliding. The dynamics imposed by the guidance is used for the control synthesis, which is based on the Lyapunov theory on stability.
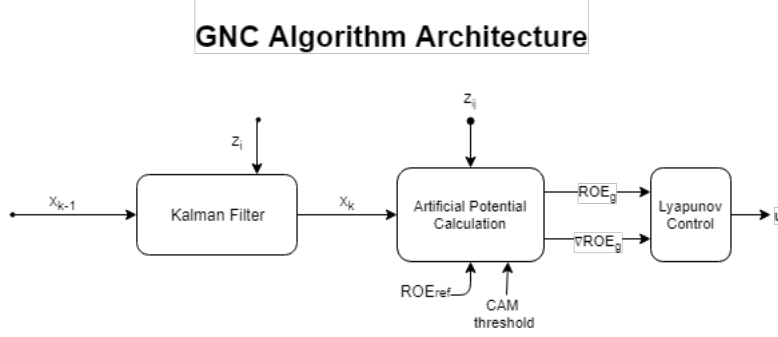
Fig. 1 GNC algorithm architecture on-board satellite *i*.

4 Numerical Simulations

In order to verify the effectiveness of the proposed algorithm, two reconfiguration scenarios are tested. Four spacecrafts flying in formation, one of which located along the reference Earth-centered orbit, reconfigure from an initial configuration to desired final one. Two different scenarios are presented, namely one reconfiguration without a collision avoidance task execution and one involving a trajectory correction by two satellites of the formation. The GNC algorithm works with a frequency of 1 Hz. The term time step refers to the fundamental update time of the loop: 1 *s*.

The final configuration is assumed to be reached with an accuracy of 1% with respect to the reference value. This threshold has been set to obtain a criterion to end the simulation. The reconfiguration algorithm is not necessarily identical to the formation maintenance one, hence it can be regarded as a limit to the reconfiguration maneuver itself. The measurements errors are assumed to be $10^{-1}m$ and $10^{-3}m/s$, in position and velocity respectively. The multiple agents are named by sequential number, namely SC1, SC2, SC3 and SC4.

4.1 Reconfiguration without Collision Avoidance Maneuver

The initial and the desired final configuration of the formation are represented by the relative orbital elements of each satellite with respect to the reference orbit. The reference orbital parameters and the spacecrafts $\delta\chi$ for initial and final configuration are summarized in Tab. 1 and 2. The reference orbit is a Low-Earth Orbit (LEO): $a = 6578 \ km$, $e = 10^{-5}$, $i = 8^o$, $\omega = \Omega = \nu = 0^o$. The reference orbits are also used to generate relative measurements by adding a fictitious noise, representative of realistic sensors uncertainty. In particular, the noise level associated to relative

position and velocity measurement respectively, is described by a Gaussian distribution with standard deviation $\sigma_{pos} = 10^{-1}m$ and $\sigma_{vel} = 10^{-3}m/s$. Spacecraft S/C 1 behaviour is not reported for analysis as it is assumed to be controlled and to follow the reference orbit.

The reconfiguration is essentially an inversion of the relative inclination vector. The component δi_x, see Eq. 1, is actually the algebraic difference of the spacecraft orbital inclination. Hence, the reconfiguration shown in this section is equivalent to an inclination change maneuver. Such reconfiguration has been chosen because of its complexity on control, involving along-radial-cross track control.

Table 1 Relative orbital elements of each spacecraft in the initial configuration

$a\delta\chi^a[m]$	S/C 1	S/C 2	S/C 3	S/C 4
$a\delta a$	0	0	0	0
$a\delta\lambda$	0	0	0	0
$a\delta e_x$	0	200	400	600
$a\delta e_y$	0	300	600	900
$a\delta i_x$	0	500	500	500
$a\delta i_y$	0	0	0	0

[a] dimensional using the semimajor axis of the reference orbit

Table 2 Relative orbital elements of each spacecraft in the final configuration

$a\delta\chi^a[m]$	S/C 1	S/C 2	S/C 3	S/C 4
$a\delta a$	0	0	0	0
$a\delta\lambda$	0	0	0	0
$a\delta e_x$	0	200	400	600
$a\delta e_y$	0	300	600	900
$a\delta i_x$	0	-500	-500	-500
$a\delta i_y$	0	0	0	0

[a] dimensional using the semimajor axis of the reference orbit

Fig. 2 shows the trajectories followed by the spacecrafts during the reconfiguration, as well as the initial and final status. The duration of the simulations is 15.93 orbits, equivalent to $T_{sim} = 84621\ s$. Again, the maneuver is considered fulfilled when the accuracy threshold of 1% is achieved. The reconfiguration is not constrained in time, but rather in the maximum achievable thrust $\mathbf{F}_{max} = (1,1,1)\ mN$. The latter constraint is assumed to be a realistic value for microsatellites implementation. The artificial potential is determined in the space of the relative orbital elements: by changing the relative eccentricity and inclination vector the formation remains bounded with respect to the natural dynamics. This, as mentioned in section 3.2, is exploited by the algorithm to construct forced trajectories that are in accordance with natural stable and bounded relative orbits. As shown in Fig. 2, it is clear
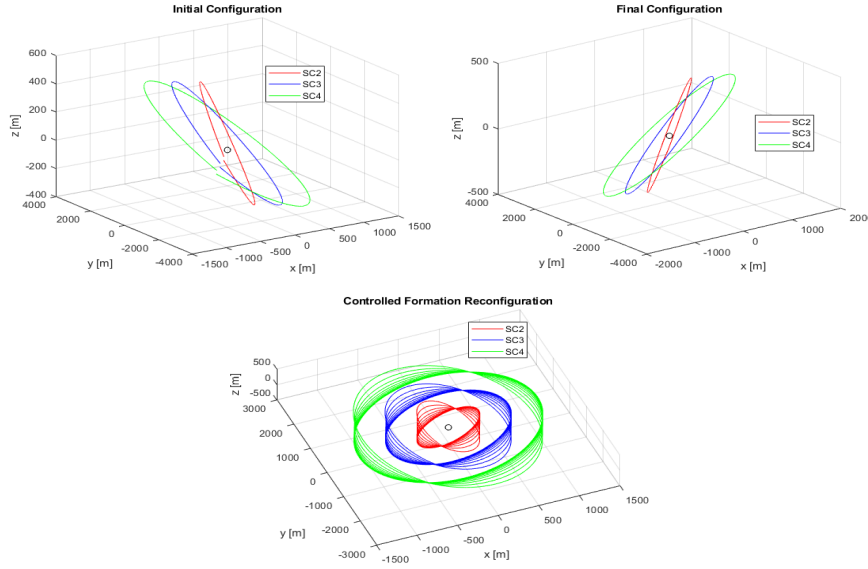
Fig. 2 Details of the spacecraft formation reconfiguration. The initial and final configuration are shown above, while below the transition is shown.

that the satellites pass from one bounded orbit to another one pushed by the artificial potential field in the ROE space. As shown in Fig. 3, the guidance algorithm provides the desired $\delta\chi$ vector at each time step. The different parameters listed in section 3.2 and 3.3 provides several degrees of freedom impacting the stability and the execution time of the maneuvers. The control law developed in section 3.3 targets the stability and convergence of the system. The control action, shown in Fig. 8 exhibits non-zero values at the stable reconfiguration point due to the presence of disturbances, which need to be counteracted for the unperturbed analytical solutions found using the model in section 2. The total Δv required by the maneuver is reported in Tab. 5. Such values of Δv are complaint with what can be generated by the propulsion system for microsatellites.

Table 3 Total 3-axis Δv required for the maneuver. Maneuver time: $T_{sim} = 84621s$.

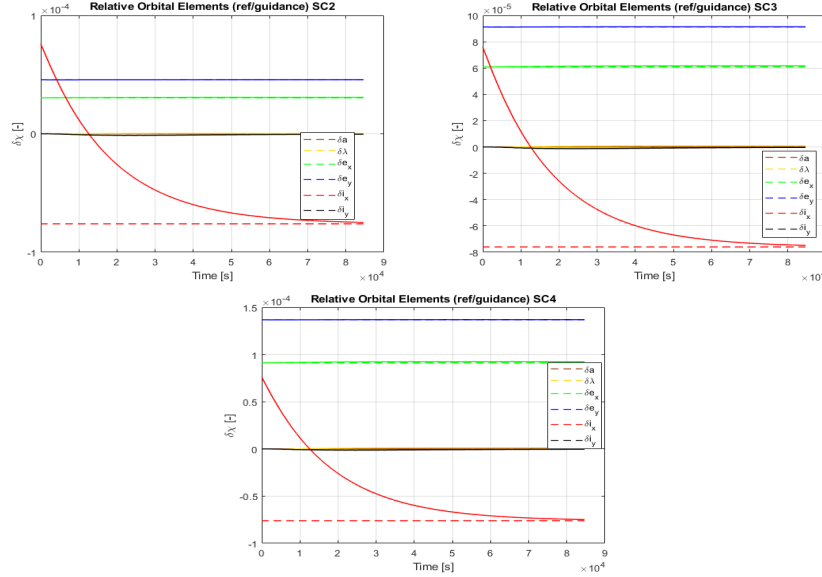|	$\Delta v_x \left[\frac{m}{s}\right]$	$\Delta v_y \left[\frac{m}{s}\right]$	$\Delta v_z \left[\frac{m}{s}\right]$
SC2	0.09	0.03	1.51
SC3	0.24	0.07	1.51
SC4	0.38	0.10	1.51

Fig. 3 The evolution of the relative orbital elements as the reconfiguration occurs. The dotted lines represent the relative orbital elements of the final configuration. The spacecraft S/C 1 is not reported because it is assumed to follow the controlled reference orbit.

4.2 Reconfiguration with Collision Avoidance Maneuver

The initial and the desired final configuration of the formation are represented by the relative orbital elements of each satellite with respect to the reference orbit. The reference orbital parameters and the spacecrafts $\delta\chi$ for initial configuration are summarized in Tab. 4. The reference orbit is a Low-Earth Orbit (LEO): $a = 6578$ km, $e = 10^{-5}$, $i = 8^o$, $\omega = \Omega = \nu = 0^o$. The reference orbits are also used to generate relative measurements by adding a fictitious noise, representative of realistic sensors uncertainty. In particular, the noise level associated to relative position and velocity measurement respectively, is described by a Gaussian distribution with standard deviation $\sigma_{pos} = 10^{-1}m$ and $\sigma_{vel} = 10^{-3}m/s$. Spacecraft S/C 1 behaviour is not reported for analysis as it is assumed to be controlled and to follow the reference orbit. The reconfiguration is specifically designed to include a collision avoidance maneuvers for the sake of demonstration. Basically, the agents 2, 3, 4 are asked to swap relative orbits with respect to spacecraft one, once again fixed along the reference orbit. The threshold d_{lim} in equation 17 is set to 50 m and an exit condition for the simulation due to collisions is set to 10 m. In particular, the maneuver is:

$$\delta\chi_{ref,2} = \delta\chi_{0,3}, \; \delta\chi_{ref,3} = \delta\chi_{0,4}, \; \delta\chi_{ref,4} = \delta\chi_{0,2}, \tag{27}$$
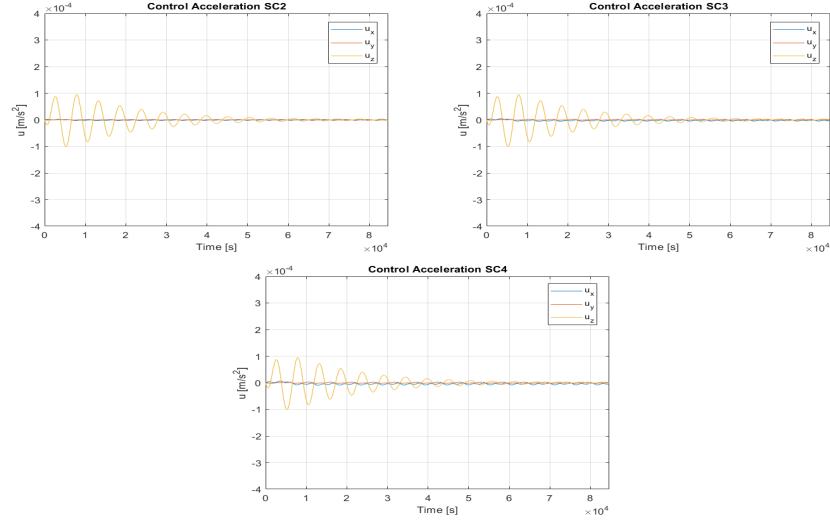
Fig. 4 The control action for the maneuvering spacecraft, namely 2,3 and 4. The cross-track component is the most relevant, since the reconfiguration deals with changes in orbital inclination.

Table 4 Relative orbital elements of each spacecraft in the initial configuration

$a\delta\chi^a$[m]	S/C 1	S/C 2	S/C 3	S/C 4
$a\delta a$	0	0	0	0
$a\delta\lambda$	0	0	0	0
$a\delta e_x$	0	200	400	600
$a\delta e_y$	0	300	600	900
$a\delta i_x$	0	0	0	0
$a\delta i_y$	0	10	10	10

[a] dimensional using the semimajor axis of the reference orbit

   Fig. 5 shows the trajectories followed by the spacecrafts during the reconfiguration, as well as the initial and final status. The duration of the simulations is 17.77 orbits, equivalent to $T_{sim} = 94368$ *s*. Again, the maneuver is considered fulfilled when the accuracy threshold of 1% is achieved. The reconfiguration is not constrained in time, but rather in the maximum achievable thrust $\mathbf{F}_{max} = (1,1,1)$ *mN*. The latter constraint is assumed to be a realistic value for microsatellites implementation. The artificial potential is determined in the space of the relative orbital elements: by changing the relative eccentricity and inclination vector the formation remains bounded with respect to the natural dynamics. When the relative distance between two agents is less than the required threshold, the active collision avoidance algorithm is activated. The global potential is consequently calculated based on the attractive and repulsive contribution, which becomes relevant only when the satellite are drawing near. The artificial potential is expressed in the Cartesian space and subsequently transformed to the $\delta\chi$ space. As shown in Fig. 6, the guidance
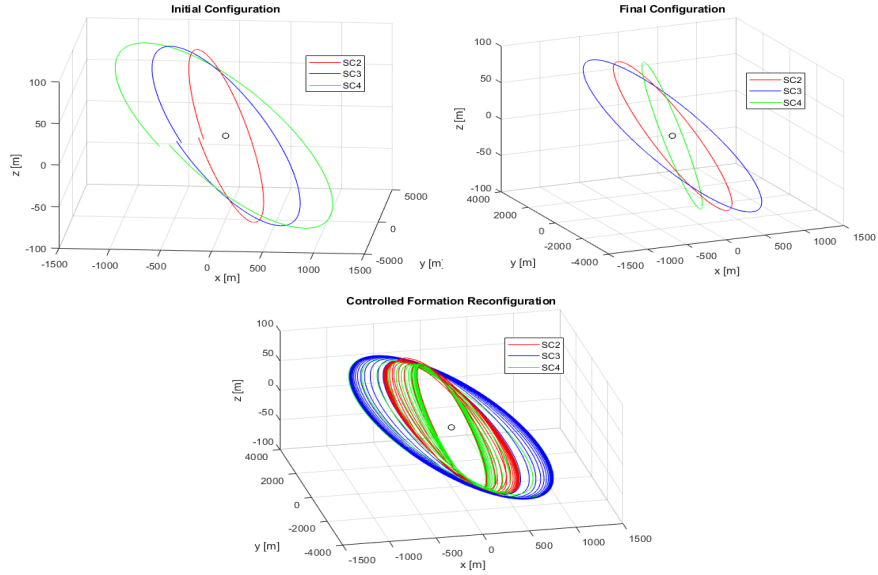
Fig. 5 Details of the spacecraft formation reconfiguration with the collision avoidance maneuver. The initial and final configuration are shown above, while the transition below.

algorithm provides the desired $\delta\chi$ vector at each time step. The algorithm provides a successful strategy to avoid the collision between the agents, which can be seen at $t \sim 2\cdot 10^4\ s$, where the attractive potential is perturbed by the repulsive contribution. The relative distances shown in Fig. 7 show how the collision avoidance maneuver prevent the satellites from getting closer than the safety boundary of 20 m. The control law developed in section 3.3 targets the stability and convergence of the system. The control action, shown in Fig. 8 exhibits non-zero values at the stable reconfiguration point due to the presence of disturbances, which need to be counteracted for the unperturbed analytical solutions found using the model in section 2. The control action required to avoid the collision between two spacecrafts, in particular SC2 and SC4, imposes a significant thrust along the radial direction. The integral of the control profile, which is directly expressed as Δv of the maneuver, is significantly impacted by the CAM maneuver, meaning that the active collision avoidance imposes a further requirement on the Δv budget. The total Δv required by the maneuver is reported in Tab. 5. Such values of Δv are complaint with what can be generated by the propulsion system for microsatellites.
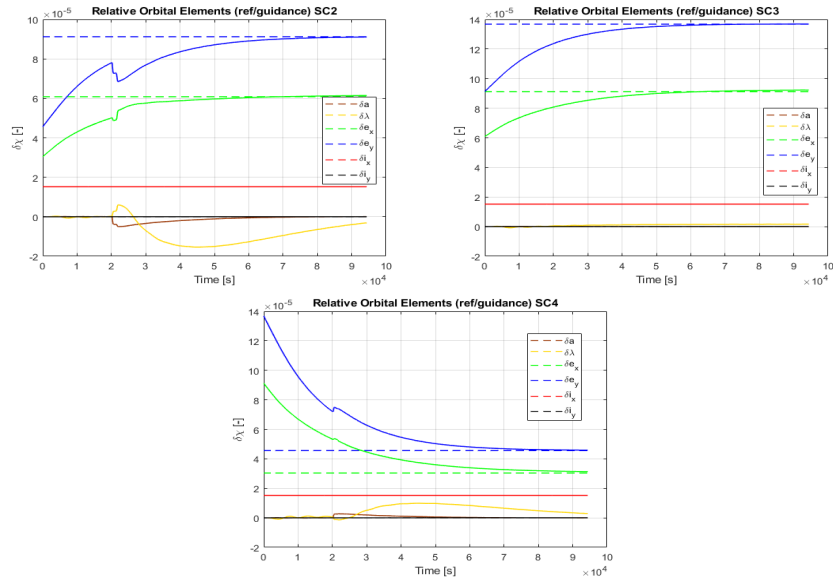
Fig. 6 The evolution of the relative orbital elements as the reconfiguration occurs. The dotted lines represent the relative orbital elements of the final configuration. The spacecraft S/C 1 is not reported because it is assumed to follow the controlled reference orbit. The collision avoidance maneuver can be clearly seen at $t \sim 2 \cdot 10^4 \ s$.
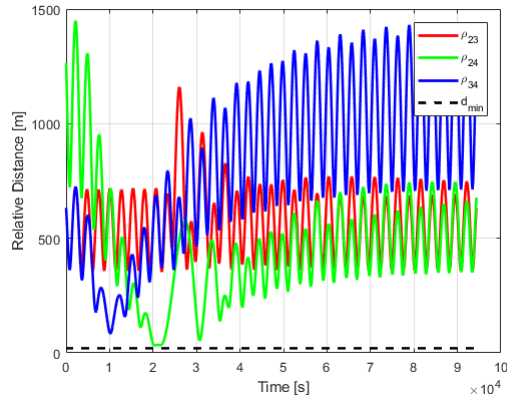

Fig. 7 Relative distance evolution between agents. The green line shows the relative distance between SC2 and SC4 that performs a collision avoidance maneuvers when approaching the minimum safe separation of 20 m.

5 Conclusions

Distributed space systems are foreseen to be the new trend for space mission. Such missions will require GNC algorithms that are more flexible and less computation-
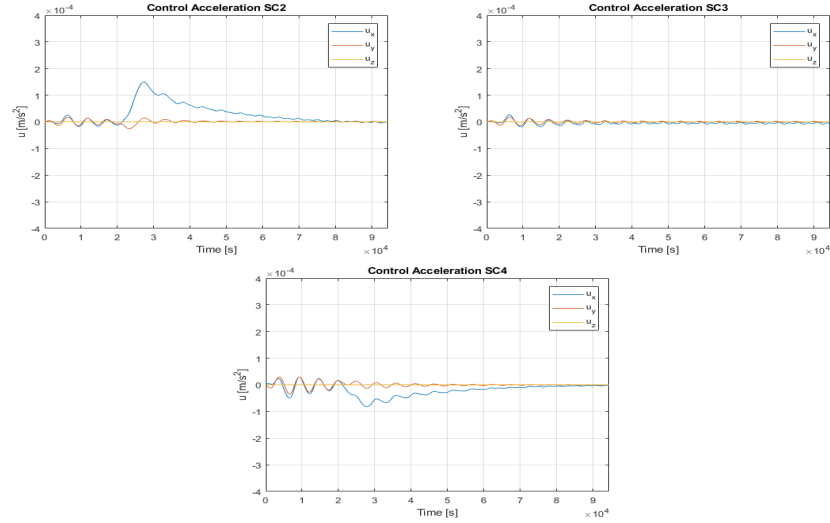
Fig. 8 The control action for the maneuvering spacecraft, namely 2,3 and 4. The control action is contained in the along-track/radial plane. The avoidance maneuver imposes a sudden control action along the radial direction.

Table 5 Total 3-axis Δv required for the maneuver. Maneuver time: $T_{sim} = 94368\ s$.

	$\Delta v_x\ \left[\frac{m}{s}\right]$	$\Delta v_y\ \left[\frac{m}{s}\right]$	$\Delta v_z\ \left[\frac{m}{s}\right]$
SC2	2.84	0.37	0.03
SC3	0.59	0.2780	0.03
SC4	2.08	0.51	0.03

ally demanding with respect to those available in literature. This paper addresses the aforementioned need by proposing a full GNC algorithm architecture for formation flying spacecraft reconfiguration. The algorithm relies on a decentralized KF, which processes relative state measurements with respect to the reference orbit. The guidance algorithm is based on the APF approach, which implements an active collision avoidance constraint based on a repulsive field expressed in the ROE space. The linear mapping between ROE and Cartesian states is derived for eccentric orbits; this is necessary because the relative trajectory acquisition is usually based on Cartesian measurements whereas the proposed algorithm relies on ROE. The main contribution of this paper is the development of a complete GNC architecture able to manage spacecrafts low-thrust reconfiguration in J2-perturbed orbits, respecting the collision avoidance constraint. The guidance algorithm presented in this paper targets flexibility and limits the computational burden for the on-board systems; on the other hand, precision and accuracy of the final desired relative orbits are assured by a distributed control law. The GNC loop has been validated through numerical simulations: in particular, one is designed to demonstrate the effectiveness of the

active collision avoidance approach. These simulations demonstrate to provide safe reconfiguration paths to multiple spacecrafts in close proximity at minimal actuation and computation cost. In particular, relative inclination reconfiguration and position swapping can be achieved with $\Delta v \sim 1\frac{m}{s}$ within ~ 1 day. Additionally, autonomous collision-avoidance path planning is performed on-board, yielding a prompt response to the hazard at a low-computational cost. The proposed algorithm does not solve the task of relative location assignment that, in presence of a swarm of identical satellites, may lead to more fuel-efficient trajectory planning. Future work will also focus on refining the collision avoidance hierarchy by generating a decision scheme in order to determine the most-performing actions between having a single spacecraft maneuvering or both.

References

1. Chernick, M., DAmico, S.: New Closed-Form Solutions for Optimal Impulsive Control of Spacecraft Relative Motion. Journal of Guidance, Control, and Dynamics. **41**, 301–319 (2016)
2. Chu, J.: Dynamics, Distributed Control And Autonomous Cluster Operations Of Fractionated Spacecraft. PhD Thesis, TU Delft (2015)
3. D'Amico, S.: Autonomous formation flying in low earth orbit. PhD Thesis, TU Delft (2010)
4. Delpech, M., et al. RF based navigation for Prisma and other formation flying mission in Earth orbits. Advances in the Astronautical Sciences, **135.2** (2009): 1533-1551.
5. Di Mauro, G., Spiller, D., Bevilacqua, R., Curti, F.: Optimal Continuous Maneuvers for Satellite Formation Reconfiguration in J2-perturbed Orbits. 2018 Space Flight Mechanics Meeting. **216**, 1–20 (2018)
6. Guffanti, T., D'Amico, S., Lavagna, M.: Long-term analytical propagation of satellite relative motion in perturbed orbits. Advances in the Astronautical Sciences, **160**, 2387-2417 (2017)
7. Izzo, D., Pettazzi, L.: Autonomous and Distributed Motion Planning for Satellite Swarm. Journal of Guidance, Control, and Dynamics. **30**, 449-459 (2007)
8. Koenig, A. W., Guffanti, T., DAmico, S.: New State Transition Matrices for Spacecraft Relative Motion in Perturbed Orbits. Journal of Guidance, Control, and Dynamics, **40**, 1749-1768 (2017)
9. Lane, C. M., Axelrad, P.: Formation Design in Eccentric Orbits Using Linearized Equations of Relative Motion. Journal of Guidance, Control, and Dynamics, **29**, 149-160 (2006)
10. Ren, W., Beard, R.: Decentralized Scheme for Spacecraft Formation Flying via the Virtual Structure Approach. Journal of Guidance, Control, and Dynamics, **27**, 73-82 (2004)
11. Schaub, H., Vadali, S., Junkins, J., Alfriend, K.: Spacecraft Formation Flying Control Using Mean Orbit Elements. Journal of the Astronautical Sciences. **48**, 69–87 (2000)
12. Schaub, H., Alfriend, K.: Hybrid Cartesian and Orbit Element Feedback Law for Formation Flying Spacecraft. Journal of Guidance, Control, and Dynamics. **25**, 387–393 (2002)
13. Schlanbusch, R., Oland, E.: Spacecraft formation reconfiguration with dynamic collision avoidance. IEEE Aerospace Conference Proceedings. 1–12 (2013)
14. Steindorf, L. M., D'Amico, S., Scharnagl, J., Kempf, F., Schilling, K.: Constrained low-thrust satellite formation-flying using relative orbit elements. Advances in the Astronautical Sciences. **160**, 3563–3583 (2017)
15. Vadali, S., Alfriend, K.: Formation Establishment, Maintenance and Control in *Distributed Space Missions for Earth System Monitoring*, 163–184 (2013)